

Effects of dilute neutron matter on the neutron star crust equation of state

G. Grams^{a,1}, J. Margueron^{b,2,3}

¹Institut d'Astronomie et d'Astrophysique, CP-226, Université Libre de Bruxelles, 1050 Brussels, Belgium

²Institut de Physique des 2 infinis de Lyon, CNRS/IN2P3, Université de Lyon, Université Claude Bernard Lyon 1, F-69622 Villeurbanne Cedex, France

³International Research Laboratory on Nuclear Physics and Astrophysics, Michigan State University and CNRS, East Lansing, MI 48824, USA

the date of receipt and acceptance should be inserted later

Abstract We develop a compressible liquid-drop model to describe the crust of neutron stars for which the role of the nuclear clusters, the neutron gas, and the electrons are clearly identified. The novelty relies on the contribution of the neutron gas, which is qualitatively adjusted to reproduce 'ab initio' predictions in dilute neutron matter. We relate the properties of dilute neutron matter to the ones of neutron stars crust and we compare the mean field approximation to an improved approach which better describes dilute neutron matter. The latter is quite sensitive to the unitary limit, a universal feature of Fermi systems having a large value of the scattering length and a small interaction range. While the impact of the accurate description of dilute neutron matter is important in uniform matter (up to 30% corrections with respect to a mean field calculations), we find a reduction of this impact in the context of the crust of neutron stars due to the additional matter components (nuclear clusters and electrons). In agreement with our previous works, dilute neutron matter is however a necessary ingredient for accurate predictions of the properties of the crust of neutron stars.

PACS 26.60.Kp Equations of state of neutron-star matter · 26.60.-c Nuclear matter aspects of neutron stars

1 Introduction

Low-density neutron matter is predicted to be quite different from ordinary nuclear matter [1,2]. Dilute neutron matter is indeed expected to be the prototype of a universal system, the so-called unitary Fermi gas.

^ae-mail: guilherme.grams@ulb.be

^be-mail: j.margueron@cnrs.fr

The unitary system was introduced by G. Bertsch in 1999 as a toy model for spin-1/2 fermions to describe low-density neutron matter [3,4] for which the effective range of the interaction r_e is smaller than the interparticle distance k_F^{-1} , which is itself smaller than the absolute value of the scattering length a_s : $r_e \ll k_F^{-1} \ll |a_s|$. In such a system, it is expected that all thermodynamical quantities are proportional to the sole remaining scale given by the Fermi momentum k_F [1]. For instance, the total energy scales with the energy of the free Fermi gas, $E = \xi_s E_{\text{FFG}}$, with $E_{\text{FFG}} = (3/5)E_F$ the energy of the free Fermi gas and E_F is the Fermi energy, $E_F = \hbar^2 k_F^2 / (2m)$. The constant ξ_s is usually called the Bertsch parameter.

Since the properties of this system are universal, cold atom gas at the unitary limit could be used to provide experimental results [5,6,7,8,9]: the universal Bertsch parameter ξ_s is measured to be 0.376 ± 0.004 [9], 0.41 ± 0.01 [7]. It has further been suggested that cold atoms may explore the whole regime from unitary to naturalness and could, therefore, provide the neutron matter equation of state (EoS) [10,11]. A recent review about neutron matter from low to high density can be found in Ref. [2].

The actual nuclear interaction is, however, not as simple as its description in the toy model [12,13]: its effective range r_e is larger than the cold atom gas one and the nuclear interaction receives contributions from angular momenta $L > 0$, which increases in size as the density increases, as illustrated for the respective S - and P -wave contributions in Ref. [14] and reported in Fig. 1. Recent predictions for the dilute neutron matter energy based on different treatments of the many-body correlations [12,14,13,15,16] are shown in Fig. 1 as well as quantum Monte-Carlo (QMC) calculation for cold atoms [12]. It is also clear in Fig. 1 that the predictions

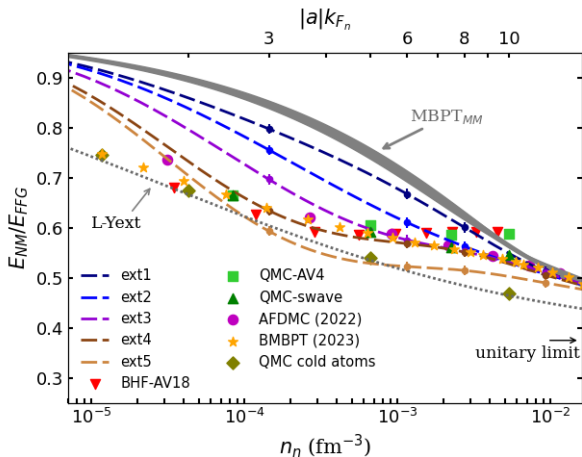


Fig. 1 Neutron matter energy normalized to the free Fermi gas energy $E_{\text{NM}}/E_{\text{FFG}}$ as function of the neutron density n_n in logarithmic scale (bottom axis) and of κ (top axis). The gray band represents the uncertainties from the mean field approximation (meta-model), which is calibrated to reproduce the many-body perturbation theory (MBPT) predictions based on several N²LO chiral-EFT interaction [17, 18]. The dashed lines represent several extensions of the mean-field approximation (ext1 to ext5), which are compared to different ‘ab initio’ predictions for dilute neutron matter shows with symbols: BHF-AV18 [13] (triangles down), QMC-AV4 [14] (squares), QMC-swave [12] (triangles up), AFDMC-2022 [15] (full circles) and BMBPT-2023 [16] (stars, cutoff $\Lambda = 2k_F$). The calculation of cold atoms is also shown as QMC cold atoms [12] (diamonds) as well as the asymptotic value for the unitary limit. Finally, the expression (2) is shown (dotted line).

for dilute neutron matter and cold atom gas are close at very low-density, but differences appear and increase as the density increases, for reasons briefly detailed here-before. Another remark is that the ratio $E_{\text{NM}}/E_{\text{FFG}}$ is close to being constant in dilute neutron matter for densities in the range 10^{-4} to about 10^{-2} fm^{-3} , but the ratio is about 0.6 instead of the value of the Bertsch constant for the unitary limit.

In a recent study, we have shown the importance of the neutron gas component for the understanding of the neutron stars crust properties by comparing different types of hamiltonians [19]. A first set of hamiltonians was based on chiral EFT interactions and a second set was aggregating predictions based on various Skyrme interactions. All these hamiltonians describe matter at the mean field approximation. We found that the small (large) dispersion in the prediction of neutron matter properties of the first (second) set could be related to the small (large) dispersion in the predictions of neutron star crust equation of state. Building upon this result illustrating the important role of the neutron gas to the neutron star crust properties, we investigate in this paper the additional effect induced by the correla-

tions in dilute neutron gas compared to the mean field predictions. In the following, we describe our treatment of these additional correlations and implement them in the modeling of the neutron star crust equation of state.

We further elaborate on the properties of Fermi systems at low-density in Sec. 2. The formalism and our results for uniform neutron matter are presented in Sec. 3, then non-uniform modeling of matter in the crust of neutron stars is described in Sec. 4 together with our results. Conclusions are presented in Sec. 5.

2 Low-density Fermi systems

Considering a N-particle quantum-mechanical system interacting via two-body hard sphere potentials at extremely low-densities Lee and Yang have obtained the following analytical expression for the energy [20],

$$\frac{E_{L-Y}}{E_{\text{FFG}}} = 1 + \frac{10}{9\pi}\kappa + \frac{4}{21\pi^2}(11 - \log 2)\kappa^2 + o(\kappa^2), \quad (1)$$

as a function of the parameter κ , which is defined as $\kappa = a_s k_F$ for cold atom gas and $\kappa = a_{nn} k_{F_n}$ for dilute neutron matter. By construction, this expression is valid only for $|\kappa| \ll 1$.

The following extension of Eq. (1) was suggested in Ref. [21],

$$\frac{E_{L-Y}^{\text{ext}}}{E_{\text{FFG}}} = 1 + \frac{10}{9\pi}\kappa \left[1 - \frac{10}{9\pi} \frac{\kappa}{1 - \xi_0} \right]^{-1}, \quad (2)$$

where the parameter ξ_0 is fixed to be $\xi_0 = 0.37$ [13] in order to reproduce cold atom gas predictions for $|\kappa| < 1$ and $|\kappa| > 1$, see Fig. 1 for instance where the relation (2) (L-Yext) is shown in dotted line and reproduce very well the cold atom gas QMC calculations.

Dilute neutron matter is known to probe the crossover region in the intermediate region between the weak (BCS) and the strong (BEC) regimes [22, 23], illustrating the importance of the residual correlations. These correlations induce superfluidity for instance, and the BCS formalism [24] could be applied in the two extreme limits of weak and strong couplings [25]. Note that the effect of pairing in Eq. (1) is ignored since it is expected to be small at extremely-low density, $E_{\text{pair}} \approx \exp(\pi/\kappa)$ [26]. While this is correct for $|\kappa| \ll 1$ and $\kappa < 0$, it may not hold true for larger values of $|\kappa|$. In the present study, we extend the Fermi gas description given in Eqs. (1) by considering the effect of correlations beyond the mean field approximation in dilute neutron matter.

To do so, the mean field description of dilute matter provided by the meta-model [27, 28] constrained by chiral EFT hamiltonians [28, 19] is taken as a reference

Table 1 Dimensionless parameters of the field Δ_n described by Eq. (5).

	ext1	ext2	ext3	ext4	ext5
a ($\times 10^{-2}$)	-1.615	-0.0322	33.59	95.94	113.1
b ($\times 10^{-6}$)	0.6784	6.589	0.0335	5.497	0.171
c ($\times 10^{-2}$)	10.95	0.704	1.236	7.420	8.137
d	1.107	2.144	2.015	1.336	1.239

and is complemented by an additional term mimicking correlations beyond mean field. This extension is calibrated such that it can be simply implemented in the modeling of the crust of neutron stars [29,30,19], see Sec. 4.

3 Dilute neutron matter

We consider spin-saturated dilute neutron matter as calculated in the following references [12,14,13,15,16] and represented in Fig. 1. Since these calculations slightly differ among each other, and we want to explore the impact of extending the mean field prediction (gray band) step-by-step, we have generated a set of extensions (ext1 to ext5) that gradually deviate from the mean field reference calculation, see Fig. 1. For this reason, extensions ext1 to ext5 are reproducing only qualitatively the 'ab initio' predictions for dilute neutron matter. Note that since pairing is not considered in the chiral EFT predictions from Ref. [17,18], we employ these results to adjust a set of meta-models reproducing the mean field approximation, see Ref. [28], which lies in the gray band shown in Fig. 1.

The energy density in dilute neutron matter is defined as $\epsilon_{\text{tot}} \equiv \epsilon_{\text{mass}} + \epsilon_{\text{int}}$, where ϵ_{mass} is the rest mass energy density for a system of neutrons and protons and the internal energy density ϵ_{int} is approximated by the following expression:

$$\epsilon_{\text{int}} \approx \epsilon_{\text{MM}} + \epsilon_{\text{corr}}, \quad (3)$$

where ϵ_{MM} is the mean field energy density given by one of the meta-model in the uncertainty band shown in Fig. 1 and ϵ_{corr} is a correction energy capturing correlations beyond the mean field approximation. Since the uncertainty in the meta-model is small, we select one of them (H2_{MM}) for the rest of the discussion. Results obtained with H2_{MM} functional provide therefore reference calculations with respect to which extensions are compared in order to evaluate the impact of the correlations in dilute neutron matter for uniform matter and for the neutron star crust equation of state.

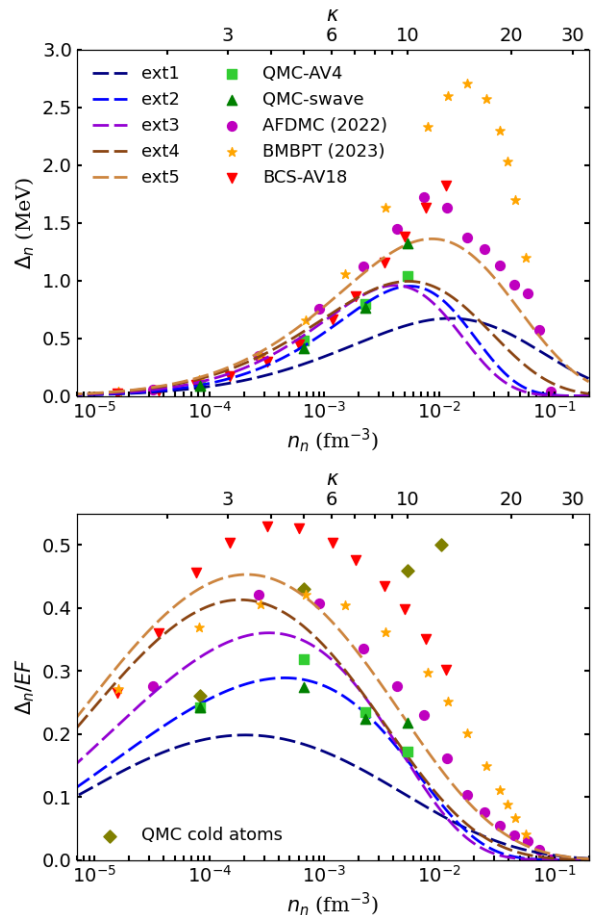


Fig. 2 Field Δ_n and 'ab initio' pairing gaps (top panel) and same quantities normalized by the Fermi energy E_F (bottom panel) w.r.t to the neutron density n_n (lower x-axis) and variable κ (upper x-axis) in neutron matter. See Fig. 1 for more details on the legend.

The correlation energy ϵ_{corr} is defined in the following way [26,31]

$$\epsilon_{\text{corr}} = -\frac{1}{2} N_{0n} (\Delta_n(n_n))^2, \quad (4)$$

where appear the density of state $N_{0n} = m_n^* k_{F_n} / (\pi^2 \hbar^2)$, the in-medium mass m_n^* , the Fermi momentum k_{F_n} defined as $n_n = k_{F_n}^3 / (3\pi^2)$, and a field $\Delta_n(n_n)$ which is adjusted to the 'ab initio' predictions for dilute neutron matter. If we replace the field $\Delta_n(n_n)$ by the pairing gap solution of the gap equation, we would obtain results similar to Ref. [13].

In the following, the field $\Delta_n(n_n)$ should not be interpreted as the pairing gap of dilute neutron matter. It mimics the effect of the many-body correlations beyond the mean field approximation in a way that makes it convenient to model the crust of neutron stars. Since the many-body correlations are expected to be large only in dilute neutron matter, the field $\Delta_n(n_n)$ is pa-

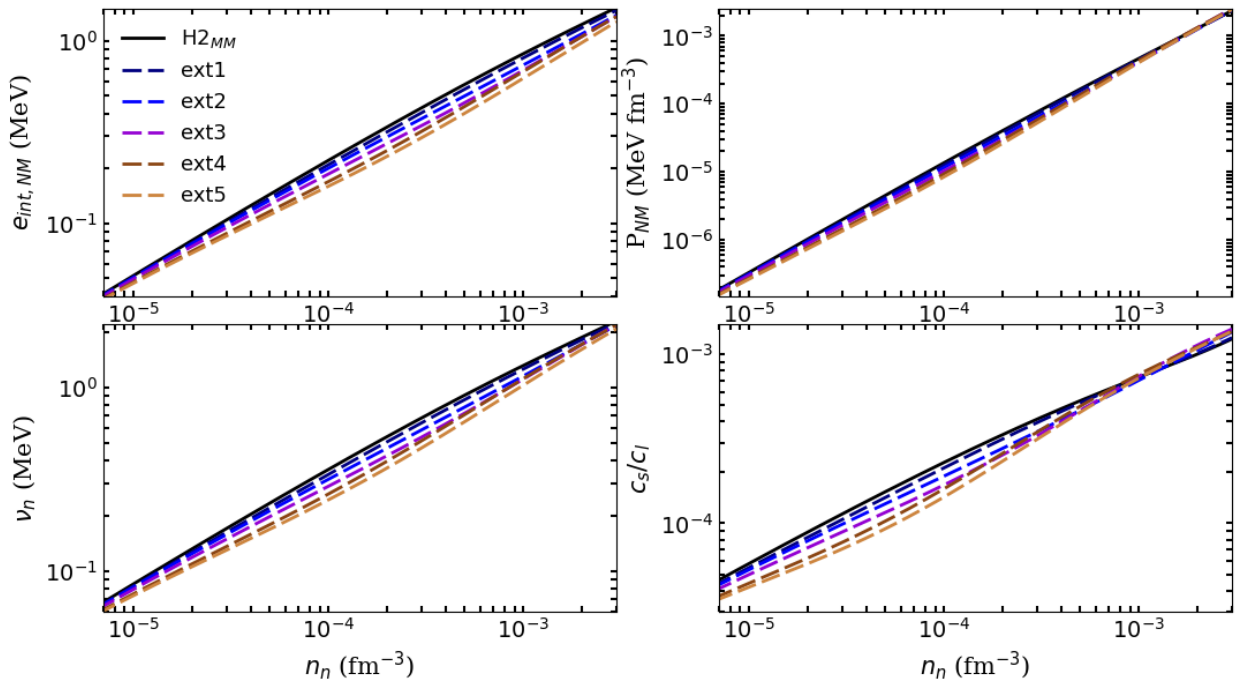


Fig. 3 Neutron matter internal energy per particle $e_{\text{int,NM}}$, pressure P_{NM} , effective chemical potential ν_n , and sound speed c_s/c_l (c_l is the speed of light in vacuum) w.r.t the neutron density n_n for H2_{MM} (solid line) and the extensions ext1 to ext5 (dashed lines).

parameterized in the following way,

$$\Delta_n(n_n) = \Delta_n^{\text{lowk}} [1 + a|\kappa|^b] \exp[-c|\kappa|^d], \quad (5)$$

where the exponential term strongly reduces the value of the field $\Delta_n(n_n)$ as the density increases, i.e., for $k_{F_n} \gg c^{1/d}/|a_{nn}| \text{ fm}^{-1}$.

The values of the four parameters a , b , c , d are given in Tab. 1 for the five extensions (ext1-ext5) represented in Fig. 1. The parameters a and b induce a polynomial correction in $|\kappa|$ to the field Δ_n^{lowk} , which at very low-density is taken to reproduce the very low-density pairing gap. This value has been derived by Gor'kov and Melik-Barkhudarov [32] and is fixed by the following analytical expression:

$$\Delta_n^{\text{lowk}} = \frac{8}{e^2} E_F \exp\left(\frac{\pi}{2\kappa} - \frac{\pi\bar{c}}{2}\right), \quad (6)$$

with the Fermi energy E_F and the constant $\bar{c} = \frac{2}{3\pi}(1 + 2 \log 2) \approx 0.506$. Note that Eq. (6) provides a value of the pairing gap at very low-density which incorporates the effects of polarization (exchange of excitations in the medium), i.e. a reduction of the low coupling pairing field, also referred as the BCS pairing gap [33, 13], by a factor of about ≈ 2 .

Note that our results are not bounded to the specific form chosen for the correlation energy (4) with the field (5). A different choice would lead to similar conclusions for dilute neutron matter.

In Fig. 2, we represent the field $\Delta_n(n_n)$ obtained for the extensions ext1-ext5 shown in Fig. 1 (dashed lines) as well as the pairing gaps obtained from the 'ab initio' calculations given in Refs. [12, 14, 13, 15, 16] (symbols). While these quantities are different in nature, they are shown to be quite similar in absolute value. The absolute values of the field $\Delta_n(n_n)$ and of the pairing gap (top panel) are scaled w.r.t. the Fermi energy E_F (bottom panel). The latter reflects more realistically the region of density where the correlations beyond the mean field approximation are expected to be stronger: in the density range between 10^{-5} and 10^{-3} fm^{-3} . The peak shown on the top panel at about $\approx 10^{-2} \text{ fm}^{-3}$ is not located in the most important region for dilute neutron matter.

We represent in Fig. 3 some thermodynamical quantities in dilute neutron matter predicted by the extensions (dashed lines) to the meta-model shown in Fig. 1: the energy per particle, the pressure, the effective chemical potential $\nu_q = (\partial\epsilon_{\text{tot}}/\partial n_q|_{\bar{q}} - m_q c^2)$, with $q = n, p$, and the sound speed. Note that we also represent the prediction of the mean field model H2_{MM} without extensions (solid line). The reduction of the energy per particle in the extended models compared to the mean field model implies a softening of the energy for densities $n_n < 10^{-3} \text{ fm}^{-3}$ and a hardening for $n_n > 10^{-3} \text{ fm}^{-3}$, which is reflected in the derivatives of the energy per particle: the pressure, the effective

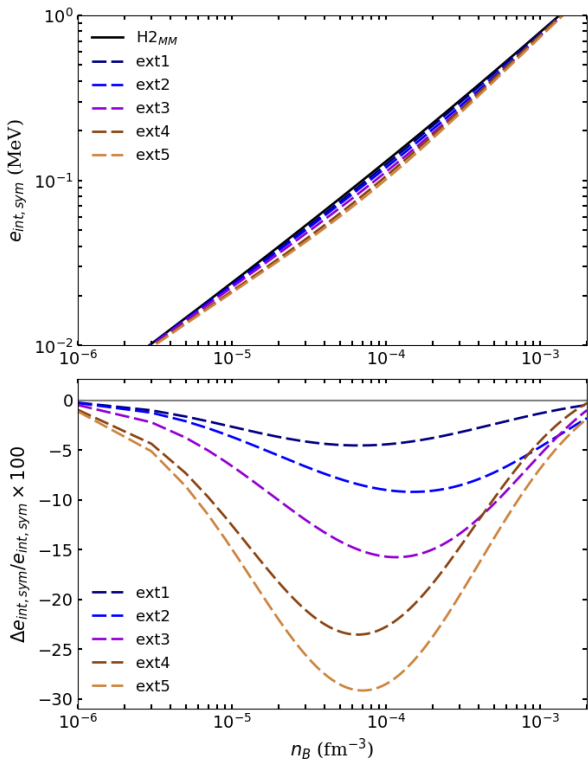


Fig. 4 Internal symmetry energy $e_{\text{int,sym}} = e_{\text{int,NM}} - e_{\text{int,SM}}$ with respect to the baryon density n_B in homogeneous matter. The relative difference $\Delta e_{\text{int,sym}}/e_{\text{int,sym}}$ reflects the difference between the prediction within the extended description of the dilute neutron matter and the prediction based on the mean field approximation. The denominator is given by the mean field approximation.

chemical potential and the sound speed (second derivative).

Note that the sound speed c_s is defined as the ratio of the incompressibility K over the enthalpy h as,

$$(c_s/c_l)^2 = \frac{K(n)}{h(n)}, \quad (7)$$

where c_l is the speed of light in vacuum, $K(n) = \partial p/\partial n$ and $h(n) = mc^2 + e(n) + p(n)/n$. Since $h(n) \approx mc^2$ at low-density, the sound speed is mostly impacted by the derivative of the pressure, as shown in Fig. 3.

The internal symmetry energy is defined as the difference between the neutron matter internal energy per particle $e_{\text{int,NM}}$ and the same value in symmetric matter $e_{\text{int,SM}}$ [28]:

$$e_{\text{int,sym}}(n) = e_{\text{int,NM}}(n) - e_{\text{int,SM}}(n). \quad (8)$$

The internal symmetry energy is shown in Fig. 4. The impact of the extensions can be important, modifying the internal symmetry energy by up to 30% at low density for $n < 10^{-3} \text{ fm}^{-3}$.

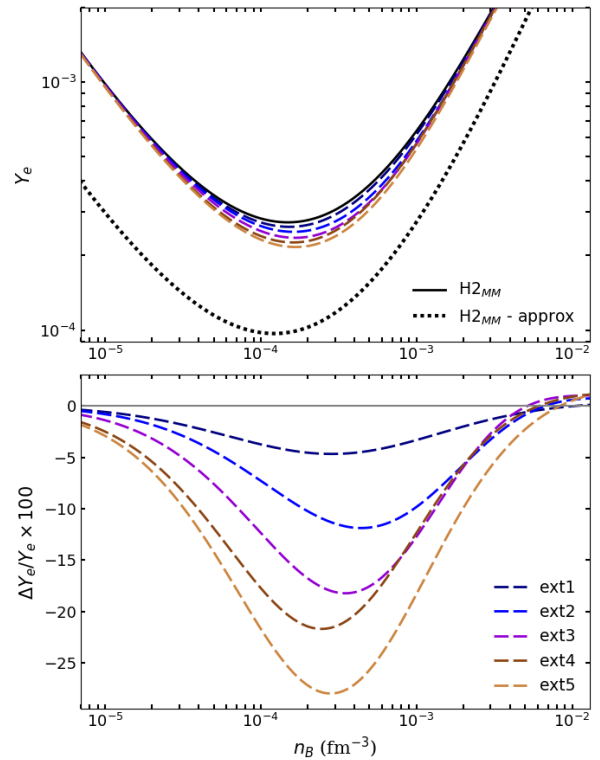


Fig. 5 Electron fraction with respect to the baryon density n_B in β -equilibrated homogeneous matter. The relative difference $\Delta Y_e/Y_e$ is calculated similarly to the one given in Fig. 4.

In Fig. 5 the electron fraction in homogeneous β -equilibrated matter is shown. As expected from the corrections to the symmetry energy, the electron fraction is also modified by a large amount, up to about 25% for $n < 10^{-3} \text{ fm}^{-3}$.

The electron fraction is obtained from the solution of the β -equilibrium equation:

$$\nu_n = \nu_p + \nu_e + \Delta mc^2, \quad (9)$$

with $\Delta mc^2 = (m_p + m_e - m_n)c^2 \approx -0.78 \text{ MeV}$. At $T = 0$ and approximating $\nu_n - \nu_p \approx 2\delta e_{\text{int,sym}}(n)$, we obtain the following expression for relativistic electrons:

$$h(3\pi^2 Y_e n)^{1/3} \approx 4(1 - 2Y_e)e_{\text{int,sym}}(n) - \Delta mc^2. \quad (10)$$

At low-density, since $Y_e \ll 1$, we obtain from Eq. (10) the following approximation:

$$Y_e \approx \frac{1}{3\pi^2 h^3} \frac{(4e_{\text{int,sym}} - \Delta mc^2)^3}{n}, \quad (11)$$

which is represented in Fig. 5 (dotted line).

In summary, the 'ab initio' predictions for dilute neutron matter, as captured by the different extensions we study, are important and can lead to substantial

corrections to the mean field predictions. The realistic case of the crust of a neutron star shall however include, in addition, the contributions from the nuclear clusters and the leptons. This is the aim of the next section.

4 Neutron star crust

The cold-catalyzed crust of neutron stars is a physical system, different from uniform matter presented in Sec. 3, that exists in nature. It is a non-uniform system containing nuclear clusters and electrons in addition to dilute nuclear matter. The respective weights of these different contributions are given by the modeling presented in this section. Note that since the uniformity of matter is broken by the sole presence of the nuclear clusters, these clusters are sometimes referred to as impurities.

In this section, we inject the dilute neutron matter description presented in Sec. 3 into a global modeling of the neutron star crust. The properties of the crust can be obtained from its reduction to a unit cell, the Wigner-Seitz cell of volume V_{WS} , surrounding a single nuclear cluster of volume V_{cl} . Matter in a mesoscopic region of the crust is assumed to be obtained by the pure replication of this geometry. We adopt the r -representation of the spherical Wigner-Seitz cell [34] schematically shown in Fig. 6: the neutron gas is treated as a uniform system occupying the total volume V_{WS} (with radius R_{WS}) minus the volume occupied by the cluster V_{cl} , while electrons fill the entire volume V_{WS} and the nuclear clusters occupy the volume V_{cl} delimited by the radial coordinate R_{cl} .

In terms of densities, the total density n_{tot} in a mesoscopic region of the crust receives contributions from the nuclear clusters n_{cl} , the neutron gas n_g , and the electrons n_e and can be written as $n_{\text{tot}} = n_B + n_e = (1 + Y_e)n_B$ with the baryon contribution

$$n_B = un_{\text{cl}} + (1 - u)n_g, \quad (12)$$

and the lepton contribution $n_e = Y_e n_B$, assuming that only electrons are present in the crust (muons appear at high densities). In Eq. (12), the quantity u is the volume fraction, which can be expressed as the ratio between the cluster volume V_{cl} over the Wigner-Seitz volume V_{WS} ,

$$u = \frac{V_{\text{cl}}}{V_{\text{WS}}} = \frac{2n_e}{(1 - I_{\text{cl}})n_{\text{sat}}}, \quad (13)$$

where we have used the electro-neutrality condition specifying that, in a Wigner-Seitz cell, the number of positive charges (Z_{cl} protons) equalizes the number of negative charges (N_e electrons): $Z = N_e$. In Eq. (13) the

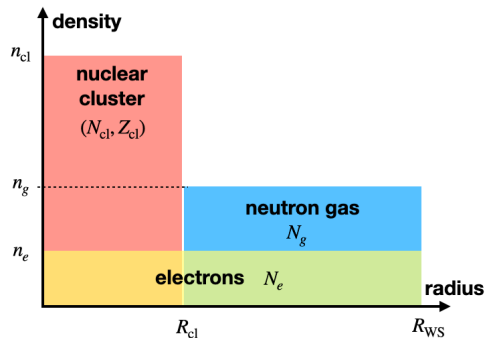


Fig. 6 Schematic description of the r -representation of the spherical Wigner-Seitz cell.

variable I_{cl} represents for the isospin asymmetry in the nuclear cluster $I_{\text{cl}} = (N_{\text{cl}} - Z_{\text{cl}})/A_{\text{cl}}$ and n_{sat} is the nuclear saturation density ($n_{\text{sat}} \approx 0.155 \text{ fm}^{-3}$ [35]).

The internal energy density in a mesoscopic region of the crust receives contributions from the different components and can be expressed as

$$\epsilon_{\text{int,crust}} = \epsilon_{\text{cl}} + \epsilon_g + \epsilon_e, \quad (14)$$

where ϵ_{cl} is the contribution of the nuclear cluster (including the contribution from the interface between the cluster and the neutron gas), ϵ_g is the neutron gas contribution (given by the modeling of dilute matter in Sec. 3) and ϵ_e is the relativistic electron contribution. The cold-catalyzed crust is approximated within the compressible liquid drop model (CLDM) with Coulomb (direct and exchange), surface and curvature terms, as detailed in Refs. [29, 30, 19]. We employ the more advanced FS4 model [30], for which the following set of non-linear and coupled stability equations are solved:

$$2E_{\text{Coul}} = E_{\text{surf}} + 2E_{\text{curv}}, \quad (15)$$

$$P_{\text{cl}} = P_g, \quad (16)$$

$$\mu_{\text{cl},n} = \mu_g, \quad (17)$$

$$\mu_{\text{cl},n} = \mu_{\text{cl},p} + \mu_e + \Delta mc^2, \quad (18)$$

$$\mu_B = \mu_g$$

$$+ \frac{2n_e}{n_{\text{cl}}A_{\text{cl}}(1 - I_{\text{cl}}) - 2n_e} \left. \frac{\partial E_{\text{surf}}}{\partial n_g} \right|_{A_{\text{cl}}, I_{\text{cl}}, n_{\text{cl}}}, \quad (19)$$

where the quantities E in Eq. (15) stand for the total energy in the Wigner-Seitz cell. Because of the non-linear and coupled nature of these equations, it is difficult to anticipate quantitatively the effect of the correlations in dilute neutron matter from the solution of these equations without correlations. The crust pres-

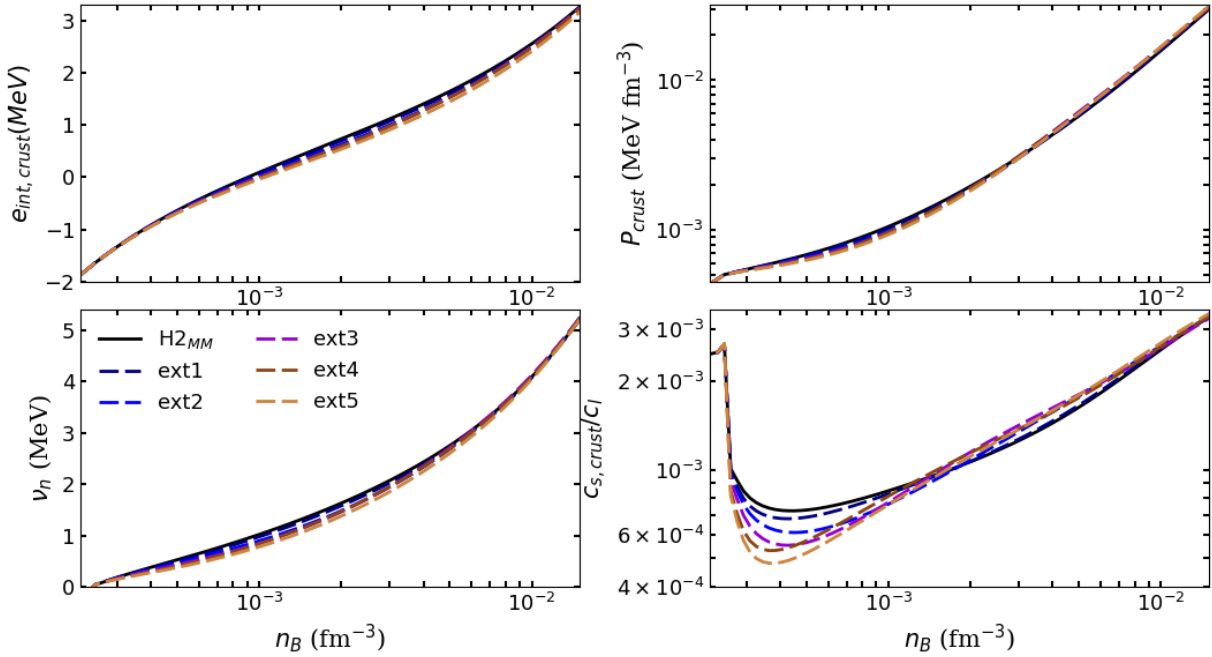


Fig. 7 Crust internal energy per particle $e_{\text{int,crust}}$, pressure P_{crust} , effective neutron chemical potential ν_n , and sound speed $c_{s,\text{crust}}/c_l$ w.r.t the baryon density n_B for H2_{MM} (solid line) and the extended models ext1 to ext5 (dashed lines).

sure and chemical potentials are defined as,

$$P_{\text{cl}} \equiv n_{\text{cl}}^2 \frac{\partial E_{\text{cl}}/A_{\text{cl}}}{\partial n_{\text{cl}}} \Big|_{A_{\text{cl}}, I_{\text{cl}}}, \quad (20)$$

$$P_g \equiv -\epsilon_g + n_g \mu_g, \quad (21)$$

$$\mu_{\text{cl},q} \equiv \mu_{\text{nuc},q} + \frac{P_g}{n_B}, \quad (22)$$

$$\mu_e \equiv \frac{\partial E_e}{\partial N_e} \Big|_{N_{\text{cl}}, Z_{\text{cl}}} + \frac{2n_e}{(1 - I_{\text{cl}})A_{\text{cl}}} \frac{\partial E_{\text{Coul}}}{\partial n_e}, \quad (23)$$

with

$$\mu_{\text{nuc},n} \equiv \frac{\partial E_{\text{nuc}}}{\partial N_{\text{cl}}} \Big|_{Z_{\text{cl}}, N_e} \text{ and } \mu_{\text{nuc},p} \equiv \frac{\partial E_{\text{nuc}}}{\partial Z_{\text{cl}}} \Big|_{N_{\text{cl}}, N_e}. \quad (24)$$

Note that the cluster chemical potentials (22) are modified by the neutron gas in the inner-crust ($P_g \neq 0$).

Results are shown in Fig. 7, where the same thermodynamical quantities as in Fig. 3 are plotted for the crust. The comparison of Figs. 3 and Fig. 7 shows the additional contribution of the nuclear clusters and the electrons. The baryon densities in Fig. 7 are chosen to span over the inner-crust, where the neutron gas density given in Fig. 3 goes from zero (at the outer-crust/inner-crust transition) to about n_B in the densest layers. Note also that since the contribution of the electrons to the density is always negligible, we have $n_{\text{tot}} \approx n_B$. The dispersion among the extensions applied to the crust and shown in Fig. 7 are smaller than the one observed in Fig. 3. This is due to the additional contribution from the clusters and the electrons which reduces the impact

of the neutron gas to the properties of the neutron star crust. The rest of our results follow the same tendency.

In the following figures, Figs. 8 and 9, we represent additional properties of the crust such as the neutron gas density n_g , electron fraction Y_e , volume fraction u , the cluster particle number A_{cl} and the Wigner-Seitz cell radius R_{WS} . While the neutron gas density and the electron fraction are almost not impacted by the energy correction in dilute neutron matter, the other properties like the volume fraction, the number of nucleons in the cluster and the Wigner-Seitz radius are more impacted.

The neutron gas density is quite insensitive to the improved modeling of dilute neutron matter because for the densities where it matters, the neutron gas density is almost identical to the baryon density n_B . The electron fraction is also weakly impacted for a different reason: Once the modeling of dilute neutron matter is well constrained by 'ab initio' predictions, the electron fraction is dominantly driven by the presence of clusters in the crust of neutron stars. In order to quantify the influence of the clusters on Y_e , the electron fraction of a uniform system without nuclear clusters and at β -equilibrium (H2_{MM}-UM) is shown in Fig. 8. This quantity was represented previously in Fig. 5 as a function of the neutron density while it is now shown as function of n_B , where the relation $n_n(n_B)$ is given by the solution of the CLDM equations. The difference observed between the curve H2_{MM}-UM and the set of curves H2_{MM}-crust illustrate the contribution of the nu-

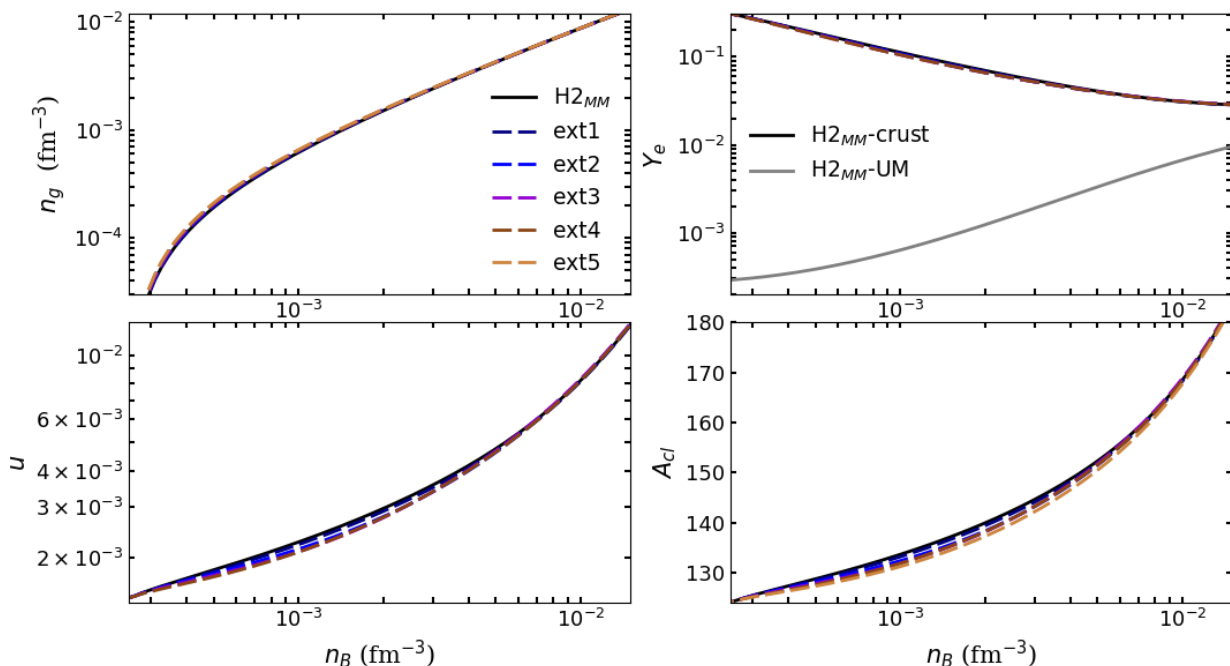


Fig. 8 Crust properties: neutron gas density n_g , electron fraction Y_e , volume fraction u and cluster particle number A_{cl} . We adopt the same notations as in Fig. 7.

clear clusters to Y_e . This explains why the quantity Y_e is very weakly impacted by the improved modeling of dilute neutron matter. We remind however that in this figure, we compare two models which are reproducing the same dilute neutron matter prediction. If this constraint is not satisfied, we then recover our previous result shown in Ref. [19]: Y_e is strongly influenced by the model for neutron matter.

Although the effect of the improved modeling of dilute neutron matter is more visible for u , A_{cl} and R_{WS} shown in Figs. 8 and 9, the relative correction remains smaller than 10%. We note for instance a 2-3% correction at maximum for R_{WS} shown in Fig. 9. In the crust of neutron star, the contribution of the improved modeling of dilute neutron matter does not seem to be a dominant effect for the results we have presented in our analysis. It is however not negligible and contributes to modify the properties of the crust up to less than 10%. Even if the effect of correlations is small, considering the important contribution from the mean field to the prediction of the equation of state in neutron star crust [19], 'Ab initio' predictions for dilute neutron matter provides important constraints.

A connection between dilute neutron matter and the crust of neutron stars has very recently been performed employing a model of phase coexistence of dense neutron-rich nuclear clusters and dilute neutron gas [36]. In such a model, the low-density component is obtained from dilute neutron matter and the high-density com-

ponent from an equation of state for uniform matter obtained from different Skyrme interactions. This model allows one to connect together different functionals specifically defined to describe dilute neutron matter or nuclear clusters. It however neglects the effect of Coulomb as well as of the interface between the nuclear clusters and the neutron gas. Even though the formalism is different between our work and the one presented in Ref. [36], results are qualitatively in agreement: the effect of the improved description of dilute matter reduce the volume fraction u , the electron fraction Y_e , the pressure P_{crust} at low density. The pressure (volume fraction) is however found to be a factor of about two larger (lower) in Ref. [36] compared to the one we calculate.

We now present more detailed results which are specific to our modeling of the crust and which cannot be obtained from a phase coexistence model, as in Ref. [36]. The number of neutrons in the gas N_g , in the nuclear cluster N_{cl} and the number of protons in the nuclear cluster Z_{cl} are shown in Fig. 10. We compare our results with other results obtained in the literature: the quantum calculation performed by Negele and Vautherin (NV) [37] (full circles), the semi-classical calculation with quantum corrections based on BSk24 Skyrme-type interaction (BSk24) [38] (stars), and the CLDM construction by Douchin, Haensel and Meyer (DHM) [39] (squares). As previously noted, although our CLDM model does not contain quantum shell ef-

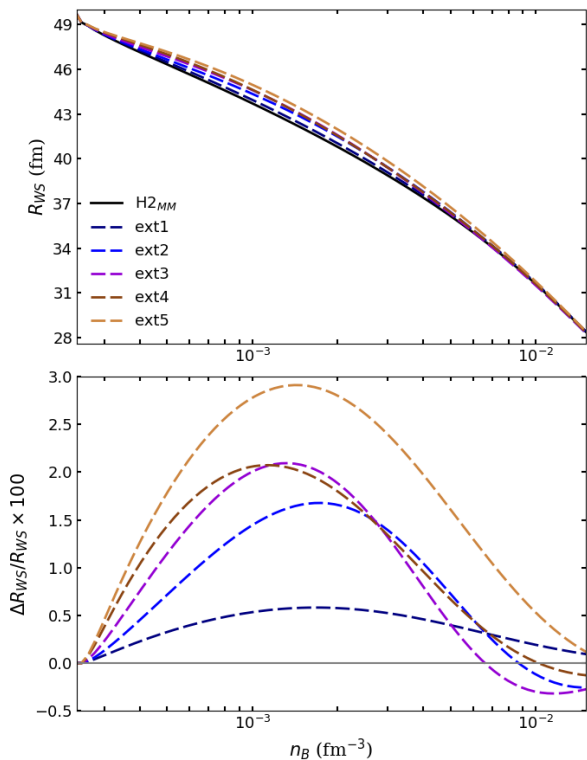


Fig. 9 Radius of the Wigner-Seitz cell in the neutron star inner-crust for $H2_{MM}$ (solid black) and the five extensions (dashed lines). The relative difference $\Delta R_{WS}/R_{WS}$ is calculated similarly to the one in Fig. 4. We adopt the same notations as in Fig. 7.

fects, it is performing quite well in predicting a quite constant value for the number of protons [30, 40].

The number of neutrons in the gas phase is the quantity which is the most influenced by the improved modeling of dilute neutron matter. It is increased by up to ≈ 60 for densities $n_B \approx 3 \cdot 10^{-3} \text{ fm}^{-3}$, which represents a correction of 8-10% to the prediction of the same quantity based on the mean field approximation. The difference between our result and other in the literature are much larger. These differences reflect the influence of the nuclear interaction itself as well as of the many-body correlations such as the shell effects. They have already been discussed, see for instance our recent analyses [29, 30, 19, 40].

Note however that there is a qualitative good agreement between our results and DHM and BSk24 concerning N_g and N_{cl} , and we are close to BSk24 concerning Z_{cl} . Note that BSk24 results are computed with the semi-classical Extended-Thomas-Fermi approach with quantum corrections added perturbatively with the Strutinsky Integral. The shell effects, which are not included in the present work, have been discussed in Ref. [40]. The large differences observed with NV results mostly originate from the nuclear interaction employed in NV

since at the moment of this work, advanced modeling of neutron matter as well as of exotic nuclei were unknown.

5 Conclusions

In this work we discuss results for dilute neutron matter constrained by 'ab initio' predictions and we estimate the impact of the accurate description of dilute neutron matter for the properties of the crust of neutron stars.

Dilute neutron matter, although strongly connected to the universal unitary limit, is not at the unitary limit. For instance, 'ab initio' predictions for the ratio E_{NM}/E_{FFG} never reach the value given by the Bertsch constant for a universal unitary gas. There are several 'ab initio' predictions for this ratio showing that it is close to a value of about 0.6 for densities $n_n \approx 10^{-4}$ - 10^{-2} fm^{-3} . Note that despite the simplicity of the interaction, there are still some differences between the different 'ab initio' calculations. We suggest a formalism that separates the mean field contribution to the one of the additional correlations. By adjusting the meta-model to the MBPT prediction in dilute neutron matter, the contribution from the mean field can be calibrated, and we suggest a set of extensions that deviate from the mean field predictions step-by-step. We label our extensions ext1 to ext5 by increasing integer reflecting the increasing differences with the mean field reference. Our largest extensions ext4 and ext5 are comparable to the 'ab initio' predictions for dilute neutron matter. We then analyze the impact of our improved modeling in dilute neutron matter and find them quite substantial: up to about 30% differences with the reference mean field prediction for some quantities and in a density region close to 10^{-3} fm^{-3} .

We obtain a quantitative estimate of the impact of dilute neutron matter predictions for the physical system that exists in nature. Reversely, measured data related to the crust can be employed to test the modeling of the crust and of its constituents, e.g., dilute neutron matter. To do so we apply our formalism to the CLDM description of cold-catalyzed neutron star crust and confront the effect of dilute neutron matter with the additional contributions from the nuclear clusters and the electrons. We obtain a large reduction of the effect of the improved modeling of dilute neutron matter, which impacts the neutron star crust properties only up to 10% or less.

We conclude our study of the relation between dilute neutron matter and neutron star crust by remarking that the correlations beyond the mean field do not dominate the properties in the crust due to the additional

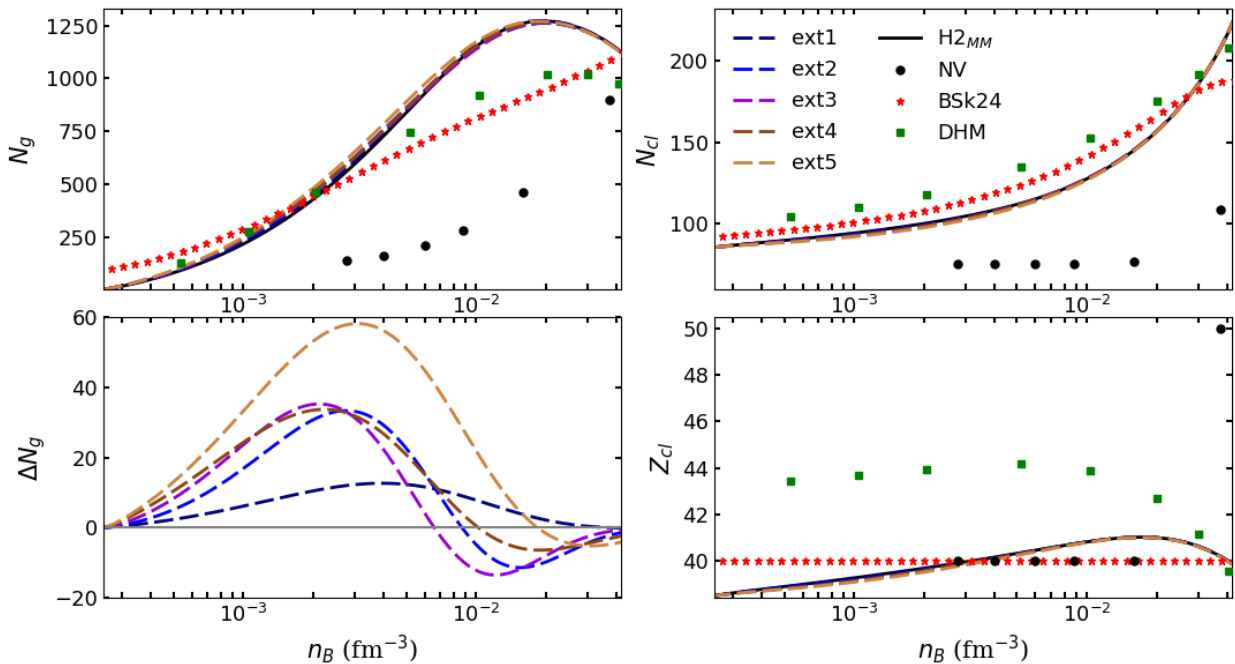


Fig. 10 Nuclear cluster properties in Wigner-Seitz cells: number of neutrons in the gas N_g , in the cluster N_{cl} and number of protons in the cluster Z_{cl} . We show predictions based on $H2_{MM}$ alone (solid line) and the extensions ext1 to ext5 (dashed lines) with the same notations as in Fig. 7. Other results from the literature are also represented: NV [37] (full circles), BSk24 [38] (stars), and DHM [39] (squares). See text for more details.

contribution of other matter components: nuclear clusters and electrons. In other words, the important effects obtained in uniform matter finally appear to be small in the physical system where dilute neutron matter is present: the crust of neutron stars. Even if this effect is small, it is important to consider globally the dilute neutron matter constraint to the equation of state in the crust of neutron stars for both the mean field and the correlation part. The mean field was discussed in a previous analysis [19]. In conclusion, dilute neutron matter remains important for quantitative calculations of the neutron star crust properties.

In the future, it would be interesting to extract additional properties in the crust of neutron stars, such as the amount of super-fluid neutrons since it influences the cooling of neutron stars [41,42], the neutron star seismology [43], the neutron star glitches [44] and possibly the release of fast radio bursts [45,46]. It would also be interesting to study finite but low temperatures in the crust of neutron stars where correlations beyond the mean field may be quenched [47,48]. The formalism presented here is well adapted for such studies, which are envisioned for future works.

Acknowledgements GG is supported by the Fonds de la Recherche Scientifique (F.R.S.-FNRS) and the Fonds Wetenschappelijk Onderzoek - Vlaanderen (FWO) under the EOS

Projects nr O022818F and O000422F. JM is supported by CNRS-IN2P3 MAC masterproject and benefits from PHAROS COST Action MP16214, as well as from the LABEX Lyon Institute of Origins (ANR-10-LABX-0066).

References

1. J. Carlson, S.Y. Chang, V.R. Pandharipande, K.E. Schmidt, Phys. Rev. Lett. **91**, 050401 (2003). DOI 10.1103/PhysRevLett.91.050401. URL <https://link.aps.org/doi/10.1103/PhysRevLett.91.050401>
2. S. Gandolfi, A. Gezerlis, J. Carlson, Annual Review of Nuclear and Particle Science **65**(1), 303 (2015). DOI 10.1146/annurev-nucl-102014-021957. URL <https://doi.org/10.1146/annurev-nucl-102014-021957>
3. G.A. Baker, Phys. Rev. C **60**, 054311 (1999). DOI 10.1103/PhysRevC.60.054311. URL <https://link.aps.org/doi/10.1103/PhysRevC.60.054311>
4. G.A. BAKER, International Journal of Modern Physics B **15**(10n11), 1314 (2001). DOI 10.1142/S0217979201005775. URL <https://doi.org/10.1142/S0217979201005775>
5. C. Lobo, I. Carusotto, S. Giorgini, A. Recati, S. Stringari, Phys. Rev. Lett. **97**, 100405 (2006). DOI 10.1103/PhysRevLett.97.100405. URL <https://link.aps.org/doi/10.1103/PhysRevLett.97.100405>
6. S. Tan, Annals of Physics **323**(12), 2971 (2008). DOI <https://doi.org/10.1016/j.aop.2008.03.005>. URL <https://www.sciencedirect.com/science/article/pii/S0003491608000432>
7. N. Navon, S. Nascimbène, F. Chevy, C. Salomon, Science **1187582** (2010). DOI 10.1126/science.1187582. URL <https://pubmed.ncbi.nlm.nih.gov/20395472/>

8. E.D. Kuhnle, H. Hu, X.J. Liu, P. Dyke, M. Mark, P.D. Drummond, P. Hannaford, C.J. Vale, *Phys. Rev. Lett.* **105**, 070402 (2010). DOI 10.1103/PhysRevLett.105.070402. URL <https://link.aps.org/doi/10.1103/PhysRevLett.105.070402>
9. M.J.H. Ku, A.T. Sommer, L.W. Cheuk, M.W. Zwierlein, *Science* **335**(6068), 563 (2012). DOI 10.1126/science.1214987. URL <https://www.science.org/doi/abs/10.1126/science.1214987>
10. P. van Wyk, H. Tajima, D. Inotani, A. Ohnishi, Y. Ohashi, *Phys. Rev. A* **97**, 013601 (2018). DOI 10.1103/PhysRevA.97.013601. URL <https://link.aps.org/doi/10.1103/PhysRevA.97.013601>
11. M. Horikoshi, M. Kuwata-Gonokami, *International Journal of Modern Physics E* **28**(01n02), 1930001 (2019). DOI 10.1142/S0218301319300017. URL <https://doi.org/10.1142/S0218301319300017>
12. A. Gezerlis, J. Carlson, *Phys. Rev. C* **77**, 032801 (2008). DOI 10.1103/PhysRevC.77.032801. URL <https://link.aps.org/doi/10.1103/PhysRevC.77.032801>
13. I. Vidaña, *Frontiers in Physics* **9** (2021). DOI 10.3389/fphy.2021.660622. URL <https://www.frontiersin.org/articles/10.3389/fphy.2021.660622>
14. A. Gezerlis, J. Carlson, *Phys. Rev. C* **81**, 025803 (2010). DOI 10.1103/PhysRevC.81.025803. URL <https://link.aps.org/doi/10.1103/PhysRevC.81.025803>
15. S. Gandolfi, G. Palkanoglou, J. Carlson, A. Gezerlis, K.E. Schmidt, *Condensed Matter* **7**(1) (2022). DOI 10.3390/condmat7010019. URL <https://www.mdpi.com/2410-3896/7/1/19>
16. V. Palaniappan, S. Ramanan, M. Urban, *Phys. Rev. C* **107**, 025804 (2023). DOI 10.1103/PhysRevC.107.025804. URL <https://link.aps.org/doi/10.1103/PhysRevC.107.025804>
17. C. Drischler, K. Hebeler, A. Schwenk, *Phys. Rev. C* **93**, 054314 (2016). DOI 10.1103/PhysRevC.93.054314. URL <https://link.aps.org/doi/10.1103/PhysRevC.93.054314>
18. C. Drischler, R.J. Furnstahl, J.A. Melendez, D.R. Phillips, *Phys. Rev. Lett.* **125**(20), 202702 (2020). DOI 10.1103/PhysRevLett.125.202702
19. G. Grams, J. Margueron, R. Somasundaram, S. Reddy, *Eur. Phys. J. A* **58**, 56 (2022). DOI 10.1140/epja/s10050-022-00706-w. URL <https://doi.org/10.1140/epja/s10050-022-00706-w>
20. T.D. Lee, C.N. Yang, *Phys. Rev.* **105**, 1119 (1957). DOI 10.1103/PhysRev.105.1119. URL <https://link.aps.org/doi/10.1103/PhysRev.105.1119>
21. D. Lacroix, *Phys. Rev. A* **94**, 043614 (2016). DOI 10.1103/PhysRevA.94.043614. URL <https://link.aps.org/doi/10.1103/PhysRevA.94.043614>
22. M. Matsuo, *Phys. Rev. C* **73**, 044309 (2006). DOI 10.1103/PhysRevC.73.044309. URL <https://link.aps.org/doi/10.1103/PhysRevC.73.044309>
23. J. Margueron, H. Sagawa, K. Hagino, *Phys. Rev. C* **76**, 064316 (2007). DOI 10.1103/PhysRevC.76.064316. URL <https://link.aps.org/doi/10.1103/PhysRevC.76.064316>
24. J. Bardeen, L.N. Cooper, J.R. Schrieffer, *Phys. Rev.* **108**, 1175 (1957). DOI 10.1103/PhysRev.108.1175. URL <https://link.aps.org/doi/10.1103/PhysRev.108.1175>
25. P. Nozières, S. Schmitt-Rink, *J Low Temp Phys* **59**, 195 (1985)
26. P.G. de Gennes, *Superconductivity of Metals and Alloys* (W.A. Benjamin Editor, New York, 1966)
27. J. Margueron, R. Hoffmann Casali, F. Gulminelli, *Phys. Rev. C* **97**, 025806 (2018)
28. R. Somasundaram, C. Drischler, I. Tews, J. Margueron, *Phys. Rev. C* **103**, 045803 (2021). DOI 10.1103/PhysRevC.103.045803. URL <https://link.aps.org/doi/10.1103/PhysRevC.103.045803>
29. G. Grams, J. Margueron, R. Somasundaram, S. Reddy, *Few-Body Systems* **62**, 116 (2021). DOI 10.1007/s00601-021-01697-y. URL <https://doi.org/10.1007/s00601-021-01697-y>
30. G. Grams, R. Somasundaram, J. Margueron, S. Reddy, *Phys. Rev. C* **105**, 035806 (2022). DOI 10.1103/PhysRevC.105.035806. URL <https://link.aps.org/doi/10.1103/PhysRevC.105.035806>
31. C.H. Yang, J. Clark, *Nuclear Physics A* **174**(1), 49 (1971). DOI [https://doi.org/10.1016/0375-9474\(71\)91002-5](https://doi.org/10.1016/0375-9474(71)91002-5). URL <https://www.sciencedirect.com/science/article/pii/0375947471910025>
32. L.P. Gor'kov, T.K. Melik-Barkhudarov, *Soviet Journal of Experimental and Theoretical Physics* **13**, 1018 (1961)
33. H. Heiselberg, C.J. Pethick, H. Smith, L. Viverit, *Phys. Rev. Lett.* **85**, 2418 (2000). DOI 10.1103/PhysRevLett.85.2418. URL <https://link.aps.org/doi/10.1103/PhysRevLett.85.2418>
34. P. Papakonstantinou, J. Margueron, F. Gulminelli, A.R. Raduta, *Phys. Rev. C* **88**, 045805 (2013). DOI 10.1103/PhysRevC.88.045805. URL <https://link.aps.org/doi/10.1103/PhysRevC.88.045805>
35. J. Margueron, R. Hoffmann Casali, F. Gulminelli, *Phys. Rev. C* **97**(2), 025805 (2018). DOI 10.1103/PhysRevC.97.025805
36. S.K. Gupta, M. Urban. Effect of the equation of state for dilute neutron matter on the composition of the inner crust of neutron stars (2023)
37. J. Negele, D. Vautherin, *Nuclear Physics A* **207**(2), 298 (1973). DOI [https://doi.org/10.1016/0375-9474\(73\)90349-7](https://doi.org/10.1016/0375-9474(73)90349-7). URL <https://www.sciencedirect.com/science/article/pii/0375947473903497>
38. J.M. Pearson, N. Chamel, A.Y. Potekhin, A.F. Fantina, C. Ducoin, A.K. Dutta, S. Goriely, *MNRAS* **481**(3), 2994 (2018). DOI 10.1093/mnras/sty2413. URL <https://doi.org/10.1093/mnras/sty2413>
39. F. Douchin, P. Haensel, J. Meyer, *Nucl. Phys. A* **665**, 419 (2000). DOI [https://doi.org/10.1016/S0375-9474\(99\)00397-8](https://doi.org/10.1016/S0375-9474(99)00397-8). URL <https://www.sciencedirect.com/science/article/pii/S0375947499003978>
40. G. Grams, J. Margueron, R. Somasundaram, N. Chamel, S. Goriely, *Journal of Physics: Conference Series* **2340**(1), 012030 (2022). DOI 10.1088/1742-6596/2340/1/012030. URL <https://dx.doi.org/10.1088/1742-6596/2340/1/012030>
41. C. Monrozeau, J. Margueron, N. Sandulescu, *Phys. Rev. C* **75**, 065807 (2007). DOI 10.1103/PhysRevC.75.065807. URL <https://link.aps.org/doi/10.1103/PhysRevC.75.065807>
42. N. Chamel, D. Page, S. Reddy, *Phys. Rev. C* **87**, 035803 (2013). DOI 10.1103/PhysRevC.87.035803. URL <https://link.aps.org/doi/10.1103/PhysRevC.87.035803>
43. N. Andersson, *Universe* **7**(1) (2021). DOI 10.3390/universe7010017. URL <https://www.mdpi.com/2218-1997/7/1/17>
44. V. Graber, A. Cumming, N. Andersson, *The Astrophysical Journal* **865**(1), 23 (2018). DOI 10.3847/1538-4357/aad776. URL <https://dx.doi.org/10.3847/1538-4357/aad776>
45. R.I. Epstein, *Physics Reports* **163**(1), 155 (1988). DOI [https://doi.org/10.1016/0370-1573\(88\)90042-7](https://doi.org/10.1016/0370-1573(88)90042-7). URL <https://www.sciencedirect.com/science/article/pii/0370157388900427>

46. Q.C. Li, Y.P. Yang, F.Y. Wang, K. Xu, Z.G. Dai, *Monthly Notices of the Royal Astronomical Society* **517**(3), 4612 (2022). DOI 10.1093/mnras/stac2596. URL <https://doi.org/10.1093/mnras/stac2596>
47. S. Burrello, M. Grasso, *Eur. Phys. J. A* **58**, 22 (2022). URL <https://doi.org/10.1140/epja/s10050-022-00665-2>
48. J. Keller, C. Wellenhofer, K. Hebeler, A. Schwenk, *Phys. Rev. C* **103**, 055806 (2021). DOI 10.1103/PhysRevC.103.055806. URL <https://link.aps.org/doi/10.1103/PhysRevC.103.055806>